Biomaterials Advances 177 (2025) 214420

Contents lists available at ScienceDirect

Biomaterials Advances

journal homepage: www.journals.elsevier.com/materials-science-and-engineering-c

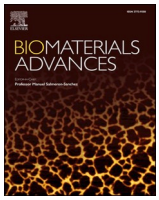

Boosted breast cancer treatment with cell membrane-coated PLGA nanocarriers: Investigating the interactions with various cell types☆

Laís Ribovski [a,b,*,1], Paula Maria Pincela Lins [b,*,1], Bruna J. Moreira [b], Luana C. Antonio [b], Juliana Cancino-Bernardi [b,c], Valtencir Zucolotto [b]

[a] Department of Biomaterials and Biomedical Technology, University Medical Center Groningen, University of Groningen, A. Deusinglaan 1, 9713 AV Groningen, The Netherlands
[b] Nanomedicine and Nanotoxicology Group, São Carlos Institute of Physics, University of São Paulo, IFSC – USP, 13566-590, São Carlos, SP, Brazil
[c] Chemistry Department, Laboratory in Bioanalytical of Nanosystems, Faculty of Philosophy, Sciences and Letters of Ribeirão Preto, University of São Paulo, 14040-901 Ribeirão Preto, SP, Brazil

ARTICLE INFO

Keywords:
Nanoparticles
Drug delivery
Cancer cell membrane coating
Cancer
Targeting

ABSTRACT

Nanomaterials inspired by nature and applied in the medical field have exhibited remarkable potential to diagnose and treat diseases. However, further improvements are required to enhance therapeutic effectiveness, particularly in terms of targeting. In this study, we formulated paclitaxel (PTX)-loaded poly lactic-*co*-glycolic (PLGA) nanocarriers (PLGA-PTX NCs) and coated with cancer cell membrane derived from MCF-7 breast cancer cells, mPLGA-PTX NCs. By leveraging the homotypic adhesion between cells, we enhance the treatment's effectiveness, which is associated with increased accumulation of mPLGA NCs in MCF-7 cells. Additionally, the cellular uptake of mPLGA NCs is investigated in cell types similar to MCF-7, which may also promote homotypic adhesion through specific adhesion molecules. This study includes A549 lung cancer cells, HDFn dermal fibroblasts, and MCF-10A non-tumorigenic breast cells. Our results show higher uptake for all cell lines, indicating homologous binding and common cell adhesion molecules, regardless of specificity. The treatment's efficacy, as evidenced by cellular metabolic activity, implies that both the percentage of NC-positive cells and uptake levels should be considered when evaluating therapeutic potency. All findings together emphasize the importance of thorough analysis of nanocarrier-cell interactions covering various cell types and understanding the nature of these interactions.

Introduction

Poly lactic-*co*-glycolic acid (PLGA) nanocarriers (NCs) are recognized delivery systems due to their biocompatibility, biodegradability, and versatility. Despite their improved delivery efficacy compared to free compounds; their outcome still needs to be improved. Particle functionalization with targeting ligands is a widely applied strategy that improves NCs adhesion and accumulation at the tumor site; in particular, overexpressed genes are targeted to achieve enhanced specificity [1,2].

Cell-cell and cell-extracellular matrix adhesion also plays an essential role in tumor progression and metastasis. Variations in adhesion, commonly regulated by changes in gene expression, facilitate the detachment of malignant cells and their attachment to new sites, leading to secondary tumors [3,4]. Exploring homotypic cell-cell adhesion offers another strategy to enhance NCs tumor accumulation. Cellular membrane material derived from immune cells [5], stem cells [6,7], red blood cells [8–10], and cancer cells present unique advantages based on their membrane properties and compositions, which are challenging to replicate synthetically [11–13]. Membrane extracts can be derived from a series of processes, including hypotonic lysis, a treatment commonly followed by mechanical disruption and ultracentrifugation. The methodology may vary depending on the type of cell used. After extraction and isolation, nanoparticles can be coated with cell membranes by different methods, e.g., ultrasonication and membrane nanoparticles coextrusion [14–16]. The isolation and coating methodology impact

☆ This article is part of a Special issue entitled: 'Advanced biomaterials' published in Biomaterials Advances.

* Corresponding authors.
E-mail addresses: l.ribovski@umcg.nl, laisribovski@gmail.com (L. Ribovski), paula.pincelalins@uhasselt.be (P.M. Pincela Lins).

[1] These authors contributed equally.

https://doi.org/10.1016/j.bioadv.2025.214420
Received 2 May 2025; Received in revised form 9 July 2025; Accepted 18 July 2025
Available online 20 July 2025

membrane quality and degree of coating which influences the interaction with cells [17].

Cancer-cell-biomimetic nanocarriers benefit from the homotypic cell adhesion between cancer cells to improve nanoparticle adhesion at the cancer site, and consequently, NCs internalization is favored [11]. Hu and colleagues were pioneers in demonstrating that polymeric nanoparticles coated with red blood cells exhibit a longer blood circulation time compared to those coated with PEG [18].

Here we focus on breast cancer, which remains one of the predominant cancers affecting women [19–21]. We propose the use of PLGA NCs containing a chemotherapy drug, paclitaxel, coated with MCF-7 cell membranes, a cell line derived from an invasive breast ductal carcinoma. The interaction of dye-loaded PLGA and membrane-coated dye-loaded PLGA NCs (mPLGA NCs) with cancerous and non-cancerous epithelial cell lines was studied using flow cytometry and confocal laser scanning microscopy (CLSM). Our findings showed increased interaction levels of mPLGA NCs for all tested cell types showing not only homotypic adhesion with the source cancer cell but also with non-cancerous breast cells, lung cancer cells and dermal fibroblasts. To assess the mPLGA NCs potential as a treatment for cancer, cell viability was tested for those same cells with systems containing paclitaxel. mPLGA-PTX NCs improved NCs specificity and efficacy against the breast cancer cell, but not against lung cancer and non-tumorigenic breast cell lines.

Materials and methods

Preparation of PTX-loaded and dye-loaded PLGA nanocarriers

PLGA NCs were prepared by the nanoprecipitation method with solvent evaporation as described in the literature by Fessi et al with some modifications [22]. Briefly, 160 μL of 5 mg mL^{-1} PTX (0.8 mg) in acetonitrile were added to 2 mL of a 10 mg mL^{-1} PLGA (Resomer 503H 50:50 MW 24000–38,000, acid terminated, #719870, Sigma-Aldrich) solution prepared in acetone and it was kept under magnetic stirring at room temperature. 6 mL of a 10 mg mL^{-1} Pluronic®-F127 (#P2443, Sigma-Aldrich) were added at once to the organic phase still under magnetic stirring (700 rpm). Following up to 5 min of magnetic stirring, acetone was evaporated under reduced pressure. NCs were centrifuged prior to use and resuspended in the appropriated solvent according to use.

To obtain fluorescent NCs, fluorescein (#F2456, Sigma-Aldrich) or curcumin-loaded NCs were prepared using a similar method as previously described, replacing PTX with either 1 mg of fluorescein dissolved in acetone or 2 mg of curcumin in DMSO. The assays that utilize the fluorescent NCs are confocal microscopy (fluorescein NCs) and flow cytometry (curcumin NCs), where different fluorophores were needed due to equipment limitation and signal intensity. After evaporation under reduced pressure, the fluorescein and curcumin-loaded NCs were centrifuged (10,000*g*, 20 min, 15 °C), resuspended in ddH_2O and placed in dialysis for 2 days, also in ddH_2O, using a dialysis membrane (14 kDa cutoff, #D9277, Sigma-Aldrich). After dialysis, the dispersion was collected, centrifuged, and resuspended in 1× PBS. These particles were employed to obtain confocal images and flow cytometry experiments. Blank nanocarriers (PLGA NCs) were prepared by the same procedure as described above except by the addition of the drug or dye to the organic phase.

Cell lines and cell culture

Human breast cancer (MCF-7), adenocarcinomic human alveolar basal epithelial (A549) and human dermal fibroblast (HDFn) cells were cultured in Dulbecco's Modified Eagle Medium (DMEM, Vitrocell or Gibco #21885025) with 10 % (*v*/v) FBS. MCF-10A cells, a non-tumorigenic epithelial cell line, were cultivated in MEBM™ Mammary Epithelial Cell Growth Basal Medium (MEBM, Lonza, #CC3151) supplemented with 100 ng mL^{-1} cholera toxin (#C8052, Sigma-Aldrich) and MEGMTM Mammary Epithelial Cell Growth Medium SingleQuotsTM Kit (Lonza, #CC4136) at 37 °C in a humidified atmosphere with 5 % CO_2. For confocal samples MCF-10A cells were cultivated in DMEM/F12 (#11330–032, Thermo Fisher) supplemented with 5 % (*v*/v) horse serum (HS, #16050122, Thermo Fisher), 20 ng mL^{-1} epidermal growth factor (EGF, Peprotech), 0.5 mg mL^{-1} hydrocortisone (#H0888, Sigma-Aldrich), 100 ng mL^{-1} cholera toxin (#C8052, Sigma-Aldrich), 10 μg mL^{-1} insulin (#I1882, Sigma-Aldrich) and 1 % (*v*/v) penicillin/streptomycin.

Cell membrane isolation

Cell membranes were isolated from MCF-7 breast cancer cell line cultivated in DMEM low glucose medium supplemented with 10 % (v/v) FBS and 1 % (v/v) Penicillin-streptomycin. At confluence, the cells were detached from the flask by trypsinization and 0.5-1 × 10^7 cells were collected and washed twice with PBS (300 g, 5 min). Then, the pellet was resuspended in hypotonic buffer (10 mM Trisbase, 10 mM NaCl, 1.5 mM $MgCl_2$, pH 6.8) and incubated for 5 min at 4 °C followed by centrifugation at 300 *g* for 5 min. The supernatant was discarded and lysis buffer (0.255 M sucrose, 20 mM HEPES, 1 mM ethylenediaminetetraacetic acid disodium salt (EDTA), pH 7.4) was added to the cells. The cell solution was homogenized using Dounce glass homogenizer or Glass homogenizer VIRTUS PII (70 cycles). To separate cell debris from membrane, the extract was centrifuged at 10000 *g* for 20 min at 4 °C. Pellet was discarded, and supernatant was spun down at 100000 *g* for 130 min at 4 °C using an ultracentrifuge Optima MAX-XP (Beckman Coulter, USA) with a TLA100.3 rotor at 4 °C. Cell membrane was suspended in 1× PBS containing 1:100 protease inhibitor cocktail (Sigma-Aldrich #8340) or SIGMAFAST™ protease inhibitor cocktail tablets according to product specifications (Sigma-Aldrich #S8830). For short-term storage, membrane extract was kept at 4 °C and for long-term storage at −80 °C.

PLGA-PTX and PLGA-dye NCs coating with MCF-7 cells membrane extract

Nanocarriers coating was performed by sonication. First, PLGA NCs were centrifuged (10,000 *g*, 20 min, 15 °C), resuspended in 1× PBS followed by 15 min sonication (80 % power, 37 Hz). Cell membrane extract was also sonicated for 15 min. Thereafter, cell membranes and PLGA NCs were mixed to dilute the NCs 10 times from the stock and sonicated for more 15 min (See Table 1). Size distribution and zeta potential (ζ-potential) of all NCs and membrane extract were evaluated using a Malvern Zetasizer Nano ZS90 instrument. To estimate the number of particles per mL as well as particle size distribution, Nanoparticle Tracking Analysis (NTA) was performed using a Nanosight NS300, Malvern.

Table 1
Z-average, PdI (polydispersity index) and ζ-potential of PLGA-PTX NCs ($n = 4$), mPLGA-PTX NCs (n = 4) and MCF-7 ($n = 1$) membrane extract were measured in 0.1× PBS (pH 7.4) and values represent mean ± SD of batches. MCF-7 was measured once by DLS. NTA size values are the mean of different batches for PLGA-PTX ($n = 2$) and mPLGA-PTX NCs ($n = 3$) as well as particles concentration. MCF-7 membrane is representative of one extraction.

	Z-average ± SD (nm)	PdI	NTA Mean (nm)	ζ-potential (mV)
PLGA-PTX	195 ± 15	0.125	170 ± 8	−5 ± 2
MCF-7 membrane	181	0.228	216	−13 ± 2
mPLGA-PTX	240 ± 63	0.206	229 ± 52	−24 ± 1

Transmission electron microscopy and cryogenic transmission electron microscopy

For transmission electronic microscopy (TEM), 3 μL of each sample was deposited on copper grids for 60 s and dried with filter paper. Samples were stained with 3 μL of 2 % uranyl acetate for 30 s and again blotted with filter paper. Cryogenic transmission electron microscopy (CryoTEM) samples were prepared using the Vitrobot Mark, Thermo Fisher by depositing 3 μL of the sample on a copper grid, the excess was blotted for 3 s with filter paper and the grid was dipped in liquid ethane. The images were obtained in JEOL 1400, in LNNano/CNPEM facilities, and JEM-2100 Transmission Electron Microscopes.

Scanning electron microscopy (SEM)

Field-emission Scanning Electron Microscopy (FE-SEM) was employed to observe NCs size distribution and morphology. Samples were prepared by drop-casting PLGA-PTX NCs diluted in ddH_2O onto clean silicon substrates and dried under reduced atmosphere. Images were collected using a ZEISS SIGMA VP field emission scanning electron microscope (FE-SEM).

Fourier-transform infrared spectroscopy (FTIR)

Fourier-transform infrared spectroscopy (FTIR) was used to analyze the differences in functional groups present in NC coated and non-coated with cell membrane extract. Samples were prepared by drop-casting copolymer PLGA, nonionic surfactant Pluronic®-F127, blank PLGA NCs, PLGA-PTX NCs and MCF-7 membrane coated PLGA-PTX NCs diluted in 1× PBS and ddH_2O onto clean silicon substrates and dried under reduced atmosphere. 128 scans were collected per sample with 4 cm^{-1} resolution from 4000 to 400 cm^{-1} using an Infrared spectrometer Nicolet 6700/GRAMS Suite.

High-performance liquid chromatography (HPLC) for paclitaxel quantification

Encapsulation efficiency (EE) was determined by HPLC. Samples were analyzed in a Waters® e2695 HPLC system equipped with the 2489 UV–Visible detector set at 227 nm. Quantification was performed at 30 °C using a Brownlee Analytical C8 column (150 × 4.6 mm, 5 μm) and a precolumn Brownlee Analytical C8 (10 × 4 mm, 5 μm) from PerkinElmer. The isocratic mobile phase consisted of acetonitrile and ddH_2O (50:50, *v*/v) and the flow rate was 1 mL min^{-1}. Method validation was performed according to the International Council for Harmonisation of Technical Requirements for Pharmaceuticals for Human Use (ICH) Q2 (R1) guidelines by the European Medicines Agency (EMEA) to evaluate linear range, limit of quantification (LOQ), precision, accuracy, selectivity and robustness. More details can be found in the Supporting Information.

PLGA NCs and PLGA-PTX NCs sample preparation for paclitaxel quantification and HPLC method validation

A volume of NCs dispersion was ultracentrifuged (100,000*g*, 120 min, 4 °C) in a Beckman Coulter Optima L-90 k, rotor SW32. Supernatant was carefully removed from the tube and the pellet was resuspended in the same volume of acetonitrile. 100 μL was transferred to a new tube and acetonitrile was evaporated under a dry nitrogen stream. The sample was resuspended in 1 mL of mobile phase (50:50 acetonitrile:ddH_2O) and filtered with 0.22 μm pore-size nylon filter. Three batches ($n = 3$) were used to determine encapsulation efficiency (see Supplementary Information, sections 1 and 2) in quadruplicate as follows

$$EE(\%) = \frac{amount\ of\ PTX\ in\ NCs}{(amount\ of\ PTX\ in\ NCs + amount\ of\ free\ PTX)} \times 100 \quad (1)$$

Cellular uptake studies by flow cytometry

Non-coated PLGA NCs and MCF-7 cell-membrane coated PLGA NCs containing curcumin as probe were used to study the effect of the membrane coating in the NCs interaction with MCF-7, A549, HDFn and MCF-10A cells. In 24-well plates, 2×10^5 cells were seeded and grown for 20–24 h. Medium was removed, and cells washed one time with 1× PBS followed by the incubation of 5×10^{10} NCs containing curcumin for 4 h in 500 μL of supplemented medium, 10^{11} NCs/mL. After incubation, medium was removed, and cells were washed twice with 1× PBS and detached by trypsinization. Samples were collected and centrifuged (500 *g*, 5 min). Finally, cells were resuspended in Sheath Fluid (#342003 BD FACSFlow™, BD Bioscience) supplemented with 0.5 % (*w*/*v*) bovine serum albumin (BSA, Fluka #05411) and kept on ice prior to flow cytometry measurements. All measurements were performed in a BD FACSCalibur™ equipped with one laser (488 nm) and excitation measured using channel FL1 (530/30). Data analysis was performed using Flowing software version 2.5.1 and Origin 9.

Confocal laser scanning microscopy

MCF-7 and MCF-10A interaction with coated and non-coated NCs was observed using a confocal laser scanning microscopy (CLSM). Cells were incubated in eight-well LabTek® chamber slide (Nalgene Nunc International) at initial seeding of 1×10^4 cells per chamber and grown for 20 h at 37 °C, 5 % CO_2. Prior to incubation, cells were washed once with 1× PBS and 5×10^{10} NCs in 200 μL of supplemented medium were incubated per well. LysoTracker™ Red DND-99 (Thermo Fisher #L7528) was incubated at 75 mol L^{-1} for 1 h with the NCs as well as Hoechst for 30 min at 1 μg mL^{-1}. PLGA-Fluorescein and mPLGA-Fluorescein NCs were incubated for 4 h at 37 °C, 5 % CO_2 in a humidified incubator. After incubation, cells were washed twice with 1× PBS, fixed with 3.7 % paraformaldehyde (PFA) for 10 min and washed again with 1× PBS. Slides were mounted with PBS:glycerol (50:50) and a cover slip was carefully placed over the samples. Image acquisition was performed on a Leica TSC SP2 confocal microscope using a 63×/1.32 immersion oil objective. *Z*-stacks were obtained with 0.2 μm intervals for PLGA-Fluorescein and mPLGA-Fluorescein NCs treated samples and 0.4 μm intervals for PLGA-NLR and mPLGA-NLR NCs treated samples. Each acquired image is composed of 512 × 512 pixels from one single frame. Samples were excited using 405 nm UV diode and excitation lasers at 488 nm (ArKr) and 543 nm (GreNe). Images were prepared using Fiji [23].

Cell viability

To evaluate if the coated NCs would be a potential and more advantageous cancer treatment compared to the non-coated NCs, PLGA-PTX NCs were prepared and their effect in cell viability was investigated by MTT viability assay after 48 h incubation. Breast and breast cancer cells from mammary gland (MCF-10A and MCF-7) were seeded at 5×10^3 cells per well, as well as adenocarcinoma lung cancer cells (A549) were seeded at 2×10^3 cells per well in 96-well plates and grown for 24 h. Prior to incubation, media was removed and 200 μL of mPLGA-PTX and PLGA-PTX NCs suspension in DMEM medium supplemented with 10 % (*v*/v) FBS were added to each well. For MCF-10A cells, NCs were in MEBM medium without horse serum as recommended by the manufacturer. After 48 h, PLGA-PTX NCs containing media were removed, cells washed twice with 1xPBS and 3-(4,5-dimethylthiazol-2-yl)-2,5-diphenyltetrazolium bromide (MTT) was incubated at 0.5 mg mL^{-1} for 4 h. Further, formazan crystals were dissolved in 100 μL of dimethyl sulfoxide (DMSO) per well and left under orbital agitation for

at least 15 min. Measurements were performed at 570 and 630 nm using a microplate reader SpectraMax M3 (Molecular Devices). Cell viability was calculated compared to controls without treatment as described in Eq. (1).

$$cell\ viability\ (\%) = \frac{(A_{570sample} - A_{630sample})}{A_{570control} - A_{630control}} \times 100 \quad (2)$$

where $A_{570sample}$ is the absorbance at 570 nm and $A_{630sample}$ at 630 nm of treated samples, while $A_{570control}$ and $A_{630control}$ represent the absorbance of non-treated samples or controls. Data analysis was performed using Origin 2020.

Results and discussion

PLGA-PTX NCs and mPLGA-PTX NCs characterization

MCF-7 membrane extracts were obtained by hypotonic lysis followed by mechanical membrane disruption using a homogenizer, and

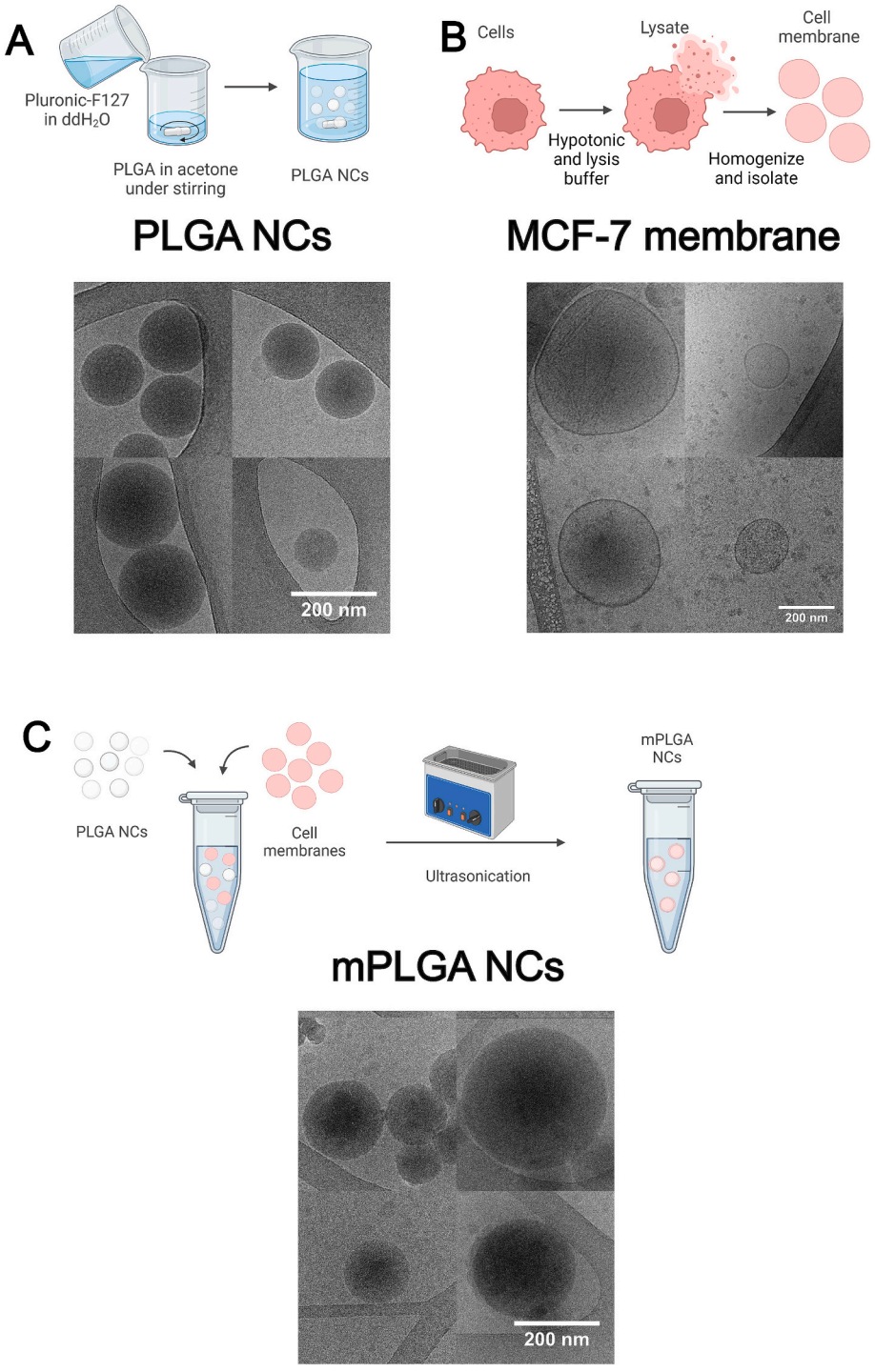

Fig. 1. Preparation and characterization of PLGA NCs coated with MCF-7 cell membranes. Schematic representation of the preparation and CryoTEM images of A) PLGA-PTX NCs B) isolated membranes of MCF-7 cells and C) mPLGA-PTX NCs in 0.1 x PBS (pH 7.4) where scale bars represent 200 nm.
(Created with BioRender.com.)

ultracentrifugation. Fig. 1 illustrates the workflow from PLGA NCs preparation and MCF-7 membrane isolation to the coating of PLGA NCs by sonication. PLGA-PTX NCs synthesis yield is at the order of high-end of 10^{12} to low-end of 10^{13} per mL. To coat the PLGA-PTX NCs with MCF-7 cell membrane, PLGA-PTX NCs were diluted 10 times, co-incubated with the MCF-7 cell membranes and sonicated. PLGA NCs and membrane-coated PLGA NCs size distributions were measured by dynamic light scattering (DLS) and Nanoparticle Tracking Analysis (NTA) (Table 1). A change in zeta potential (ζ-potential) is observed, as well as a shift in the hydrodynamic diameter, when the PLGA NCs are combined with MCF-7 membrane employing sonication (Table 1), which indicates that the NCs are coated with MCF-7 membranes.

NCs morphology was observed by transmission electron microscopy, cryogenic transmission electron microscopy (CryoTEM) and scanning electron microscopy. Scanning electron microscopy images support the monodisperse nature of PLGA-PTX NCs as represented in Fig. S3F. Negative-stain transmission electron microscopy images (Fig. S3A, S3B, S3G and S3H) illustrate the NCs spherical nature, although it was not possible to observe the membrane coating, as negative staining effects can lead to misinterpreted assumptions.

CryoTEM analysis (Fig. 1A, B and C) did not enable membrane visualization when combined with the NCs since contrast between membranes and NCs was not distinguishable (Fig. 1C). Although, it was noticeable the lack of vesicular forms in samples of mPLGA-PTX NCs (Figs. 1C and S4A) when compared to MCF-7 membrane samples (Fig. 1B) supported by the full images in the Supplementary Information, indicating the successful coating of the NCs with the membranes.

Additionally, Fourier Transform-Infrared Spectroscopy (FTIR) of copolymer PLGA, nonionic surfactant Pluronic®-F127, blank PLGA NCs, PLGA-PTX NCs and MCF-7 membrane coated PLGA-PTX NCs was performed. Fig. S3I displays FTIR spectra and permits to discriminate the mPLGA-PTX spectrum distinctive bands. Membranes are mainly composed of lipids, proteins and carbohydrates and the presence of a few characteristic bands of these components can be observed like amide I band (1650 cm^{-1}) related to C═O stretching of peptide bonds, indicative for proteins. The spectral range of 1250 to 1000 cm^{-1} indicates the existence of carbohydrates and phosphate, however, lipid phosphate head groups were excluded from analysis due to the potential interference of phosphate groups from PBS, which could cause misinterpretation of the spectra [24].

Employing a HPLC validated method (see Supplementary Information), three batches of paclitaxel-containing PLGA NCs were analyzed regarding their encapsulation efficiency (EE). Samples were prepared as described in the Materials and Methods section and EE for the three batches was 98 ± 1 % (mean ± SD).

(MCF-7)-membrane-coated PLGA NCs preferential cellular interaction over PLGA-NCs

Flow cytometry experiments were performed to evaluate the cellular uptake of cell (MCF-7)-membrane-coated and non-coated PLGA NCs. Curcumin was used as fluorescent probe. Fig. 2A shows that when incubated with membrane-coated NCs, both cancer and non-cancer cells exhibit an uptake increase, with a ratio ($MeanFluorescence_{mPLGA}$/$MeanFluorescence_{PLGA}$) greater than 1 when coated NCs were compared to non-coated NCs. When mPLGA is incubated with the source cell, MCF-7, results indicate a greater uptake, with a 1.6 ± 0.1-fold increase, compared to MCF-10A and HDFn, which showed 1.43 ± 0.05 and 1.30 ± 0.04-fold increases, respectively. Curiously, the increase for A549 is 1.63 ± 0.03, which is essentially the same as for the source cells. To account for the possibility that a shift in mean fluorescence may be caused by either high intensity events or low intensity events over different number of cells, the number of positive events for NCs (FL2+) was also evaluated. In Fig. 2B, the cell-NCs interaction is enhanced for mPLGA, however, the higher number of positive cells for A549 combined with the comparable increase in uptake indicate that each positive event has a lower amount of NCs per cell than MCF-7 cells, as illustrated in Fig. 2C.

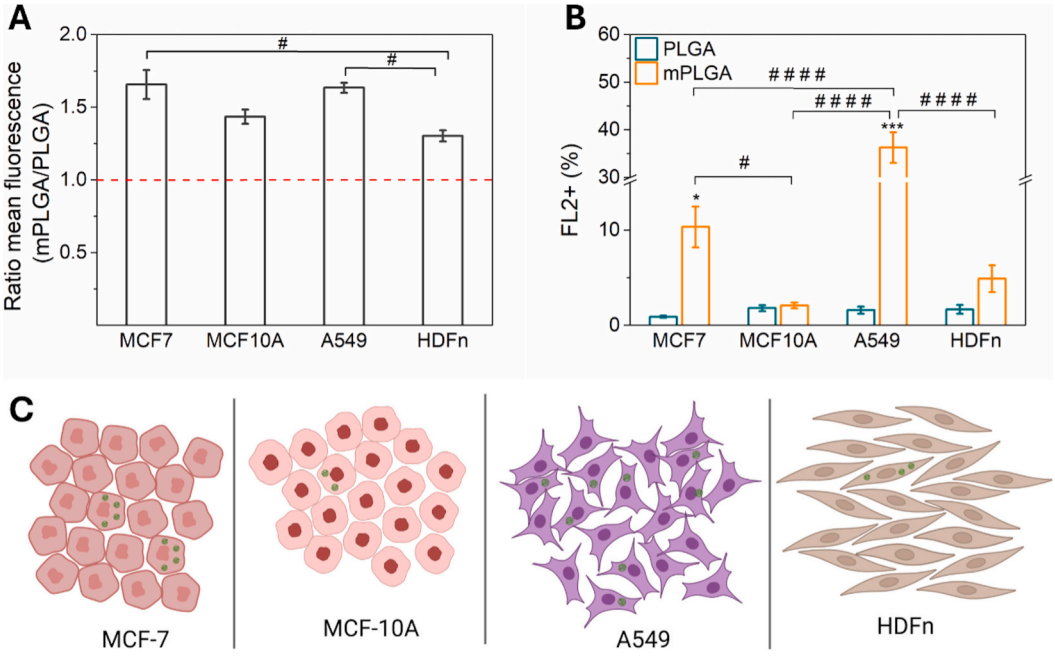

Fig. 2. Cell interaction with (MCF-7)-membrane coated and non-coated PLGA NCs by flow cytometry. A) Ratio of fluorescence mean intensity of coated (mPLGA) NCs and non-coated (PLGA) NCs, mPLGA-to-PLGA ratio, and B) percentage of NCs positive cells for mPLGA and PLGA NCs for MCF-7, MCF-10 A, A549 and HDFn incubated with NCs for 4 h. 5 × 10^{10} NCs were added per well. C) Representative scheme for the membrane-coated NCs distribution in cell populations (internalization and cell surface adhesion). Values are mean ± SE of three independent experiments. Data was analyzed by analysis of variance (ANOVA) and Tukey's post hoc test and Student *t*-test. Significance between PLGA and mPLGA NCs are indicated with * for *p*-value <0.05 and *** for p-value <0.001. Significant differences between cells: # for p-value<0.05 and # # # # for p-value <0.0001.
(Created with BioRender.com.)

The increased interaction between cancer cell-membrane coated nanoparticles and the source cell is ascribed to the cancer cells' ability to engage in homologous binding, which results in improved targetability [11,25]. mPLGA NCs higher uptake and greater percentage of NC-positive cells compared to PLGA NCs for A549, HDFn and MCF-10A cells and not only MCF-7, the source cell, suggest that adhesion plays an important role on cell membrane coated-nanoparticles technology regardless of specificity. It also suggests the involvement of common cell adhesion molecules, e.g., epithelial cell adhesion molecule (EpCAM), an overexpressed protein in epithelial-like cancers [26,27]. The intracellular domain derived from EpCAM proteolysis is implicated in the loss of contact inhibition in cancer cells leading to uncontrolled proliferation [28]. Among MCF-7, A549 and MCF-10 A, the MCF-7 cells present the highest levels of EpCAM expression, followed by A549 and MCF-10 A [27]. Changes in glycosylation pattern may also justify the increase interaction with cancer cells, for example, increase in N-glycan branching, mucin and sialyl Lewis structures [29–31]. These findings highlight the complexity of nanoparticle–cell interactions and suggest that multiple mechanisms may be involved; therefore, further investigation is required to elucidate the key mechanisms driving the enhanced uptake and interaction of membrane-coated nanocarriers.

MCF-7 membrane coated and non-coated PLGA-Fluorescein NCs were incubated with MCF-7 and MCF-10A cells at 5×10^{10} NCs per chamber for confocal microscopy analysis. Fig. 3 shows the cellular

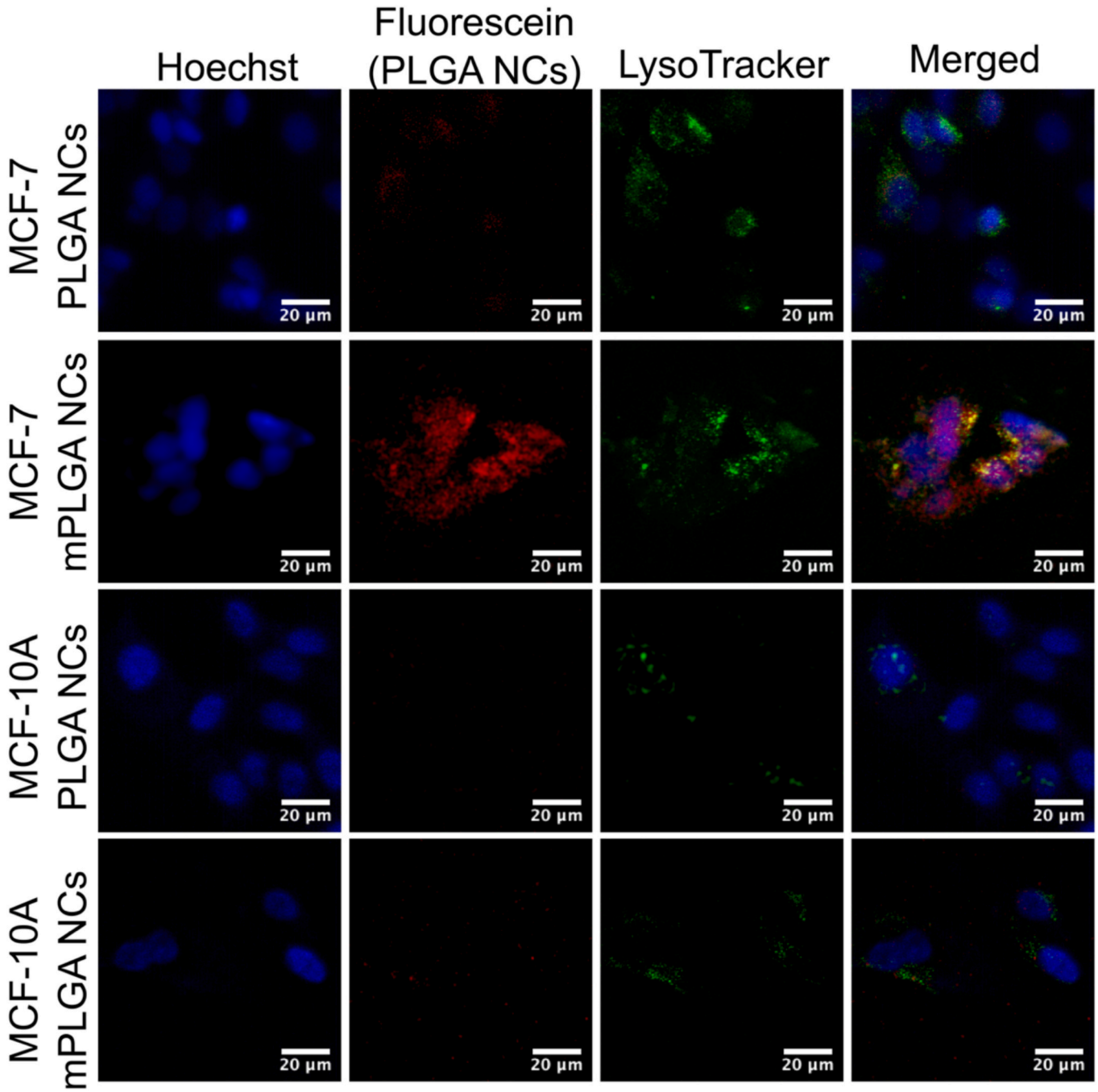

Fig. 3. Cellular interaction of (MCF-7)-membrane coated and non-coated PLGA NCs by confocal microscopy. MCF-7 and MCF-10A cells were exposed to fluorescein-PLGA or fluorescein-mPLGA NCs for 4 h at 5×10^{10} NCs per well. Cells were imaged with a 63× oil-immersion objective and acquired in z-stacks at 0.2 µm intervals. Images were acquired with the same system and laser settings.

uptake of PLGA-Fluorescein and mPLGA-Fluorescein NCs by MCF-7 and MCF-10A after 4 h incubation. The images provide evidence that the membrane coating of MCF-7 cells impacts the uptake of PLGA NCs by the MCF-7 breast cancerous and, to a lower extent, non-cancerous cells. This effect is more prominent in MCF-7 cells, as shown in Fig. 3, which supports the results obtained using flow cytometry (Fig. 2A).

In vitro evaluation of the therapeutic effect of (MCF-7)-membrane coated PLGA-PTX NCs against epithelial cell types

Building on the previous results, it is important to examine the potential of coated NCs for cancer treatment. To this end, MCF-7 (Fig. 4A) and A549 (Fig. 4B) epithelial cancer cells, HDFn dermal fibroblast (Fig. 4C) and MCF-10A (Fig. 4D) non-tumorigenic breast cells were subjected to viability evaluation after exposure to free PTX, PLGA-PTX NCs and mPLGA-PTX NCs for 48 h. Fig. 4A shows the therapeutic effect of the NCs in MCF-7 cells, the source cell for the membrane. The highest tested PTX concentration in the source cell resulted in a 1.8-fold reduction in viability from PLGA-PTX to mPLGA-PTX NCs. The results indicate that the viability of cells exposed to the free drug remained above 70 % for all concentrations. In contrast, exposure to PLGA-PTX and mPLGA-PTX NCs resulted in viability values below 70 % within the PTX concentration range of 0.75–15 ng mL^{-1}. This difference may be attributed to intracellular accumulation and the gradual release of PTX from the NCs as opposed to immediate exposure to the free drug. Likewise, the viability of A549 (Fig. 4B) and MCF-10A (Fig. 4D) cells treated with PLGA-PTX and mPLGA-PTX NCs was investigated, and no significant changes were observed. The uptake studies indicated that the increase in total for MCF-7 and A549 fluorescence associated to the presence of the membrane coating is comparable (Fig. 2A). However, in the A549 cells, the increase is distributed across a higher number of cells, meaning there are less NCs per positive event (Fig. 2C) and, consequently, less drug per cell. MTT assay is based on metabolic cellular activity, for the A549, it may be that the drug concentration per cell is insufficient to inhibit cell proliferation. Considering only positive events and relative fluorescence, the fluorescence intensity per event for MCF-7 positive events is double the fluorescence intensity compared to A549, 0.026 ± 0.003 and 0.011 ± 0.003, respectively. Comparing MCF-7 and HDFn (0.02 ± 0.01), the fluorescence per event is similar, which might explain the impact of the (MCF-7)-membrane coated NCs in HDFn cells as shown in Fig. 4C. In the case of HDFn cells, the PLGA NCs demonstrated considerable effectiveness against the cell population even without the coating, which could have contributed to the outcome as the coating provided an additional boost on top of an already effective reduction in cell viability. For MCF-10A (Fig. 4D), a non-tumorigenic breast cell line, there was an increase in the ratio mean fluorescence (Fig. 2A), but the number of positive cells was virtually unchanged (Fig. 2B). It should be highlighted that cells which the presence of the mPLGA-PTX NCs improved the treatment efficacy, MCF-7 and HDFn, also showed increase with the PLGA-PTX NCs, non-coated NCs, but the cell membrane coating boosted the outcome. Furthermore, the effective internalization of paclitaxel-loaded NCs in contrast to their adhesion to the cell membrane may also influence their effectiveness, given that paclitaxel acts on microtubules by binding to the beta-tubulin subunit [32,33].

PLGA nanoparticles coated with MDA-MB-435 cell membrane, a human melanoma cell line, have been shown to enhance binding with the MDA-MB-435 cell, the source cells, but barely any increase was observed when exposed to HFF-1, a human foreskin fibroblast cell line [11]. Likewise, our work also does not show a major increase in uptake

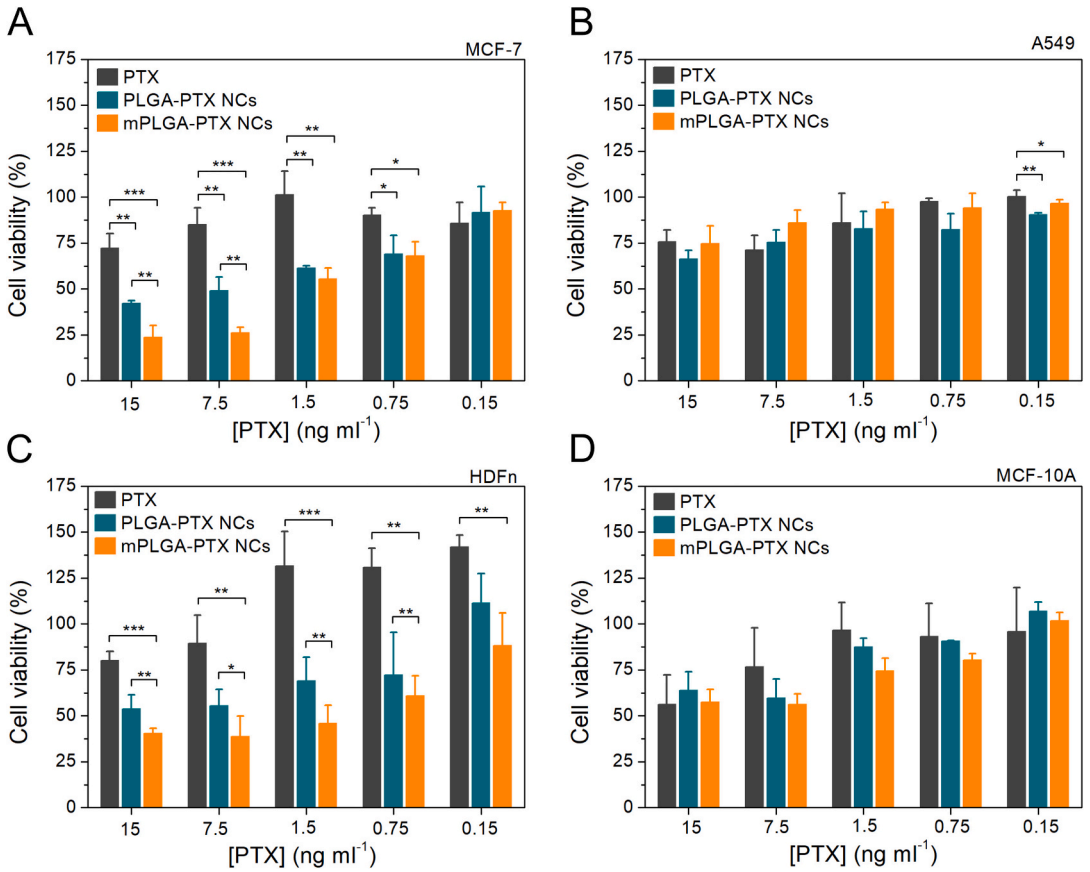

Fig. 4. Cellular viability of A) MCF-7, B) A549, C) HDFn and D) MCF-10A after 48 h incubation with different concentrations of free PTX, mPLGA-PTX and PLGA-PTX NCs evaluated by MTT viability assay. Data was analyzed using ANOVA with Tukey's post-hoc test and significances are indicated by * *p*-value <0.05, ** p-value <0.01 and *** p-value <0.001. Values are mean ± SD of three independent experiments in triplicate.

in fibroblasts but therapeutic effect was significantly different between coated and non-coated particle. Although the effect can be partially attributed to the sensitivity of those cells to the drug, it points out that there is more to the interaction than revealed solely by uptake increase.

Rao and colleagues [34] used head and neck squamous cell carcinoma patient-derived tumor cells to coat gelatin nanoparticles loaded with cisplatin. The authors demonstrate not only almost complete tumor elimination by treatment with the membrane-coated gelatin particles loaded with cisplatin, but also a favorable response against tumor recurrence in a postsurgery model. While the use of patient-derived cells would be ideal, it can be challenging to establish such technology to clinical scale as these cells must first be proliferated to reach sufficient yield before proceeding to treatment preparation. Identifying cell membrane characteristics that benefit the coated delivery system effectiveness, e.g., adhesion molecules and tissue similarities, may allow engineering or screening cells with valuable characteristics or partially matching membrane to the tumor cells that will assist the delivery and accumulation of the nanoparticles. Then, a more comprehensive assessment of nanoparticle-cells interaction is beneficial to predict side effects and effectiveness.

It is worth noting that the increased interaction with other cell types does not render the cell-membrane technology invalid. Tissue invasion is one of the classical hallmarks of cancer development together with uncontrolled cell division. Stromal cells in the tumor microenvironment also contribute to tumor development and invasiveness, including fibroblasts. These hallmarks combined with tumor heterogeneity, present a major challenge to achieving homogenous distribution of chemotherapeutics and effective tumor treatment [35,36]. The interaction between cancer-associated fibroblasts and cancer cells is heterotypic, but potentially contributes to the adhesion between cancer cell membrane-coated NCs and fibroblasts [37–39].

We suggest that cell-membrane coated nanoparticles in vitro studies take into consideration more than the targeted cells, like cancer cells, but also cells present in the microenvironment and other cells from tissues the nanoparticles might accumulate. Here we focus on epithelial cell types besides the source cell to approach if common epithelial tissue characteristics would impact delivery specificity. Specific controls will depend on the nature of the experiments; however, we advise that non-cancerous cells from the same tissue of the cancer cells, here mammary gland, should always be included for both uptake and therapeutic effect experiments. Besides, including cellular types found in multiple organs like fibroblasts, and cells present in organs with high nanoparticle accumulation, e.g., hepatic cells, are valuable controls to investigate whether an increase in NCs' specificity is being promoted more effectively, and its correlation with toxic effects. It is worth noting that fibroblasts are found in various organs, but their biomolecular fingerprint and membrane composition differ between organs [40]. Evidently, evaluating if the treatment would be effective against additional cancer cell types would be of scientific interest as well as supportive cells in the tumor microenvironment, e.g., cancer-associated fibroblasts, tumor-associated macrophages and endothelial cells. Additionally, inclusion of cells from organs with reported adverse effects caused by the free drug is crucial. One notable example is doxorubicin, which is frequently used as a model drug and induces cardiomyopathy [41,42].

Furthermore, it is advised to not only examine the uptake of nanoparticles based on intensity but also to analyze the percentage of cells positive to the NCs. The distinction between membrane association and internalization could also provide unique insights to the study. Moreover, although not addressed in this study, toxicity assessments should not be restricted solely to metabolic changes, such as MTT assay, but should also incorporate other mechanisms of damage [41,43].

Conclusions

Here we successfully developed PLGA NCs coated with MCF-7 cells membrane extracts which led to improved therapeutic efficacy against breast cancer cells. However, our findings go beyond this achievement. It also evidences the need for more comprehensive studies on the interaction between membrane-coated nanocarriers and cells, broadening beyond source cell interaction. A set of relevant cellular types should also be considered, e.g., cells associated with organs with higher nanoparticle accumulation; cells found across various organs, e.g., fibroblasts; cells with similar characteristics to the source cells, e.g., non-cancerous cells derived from the same tissue as the affected cells; and cells with a comparable membrane composition like normal epithelial cells that cover multiple organs. In addition, it is important to analyze the percentage of cells that uptake the nanoparticles, not just the increase in uptake. This work contributes to the understanding of how coated-nanocarriers interact with different cell types. Further work is required to prove the correlation and efficacy in vivo and in personalized clinical applications.

CRediT authorship contribution statement

Laís Ribovski: Writing – review & editing, Writing – original draft, Visualization, Validation, Methodology, Investigation, Funding acquisition, Formal analysis, Data curation, Conceptualization. **Paula Maria Pincela Lins:** Writing – review & editing, Visualization, Validation, Methodology, Investigation, Formal analysis, Data curation, Conceptualization. **Bruna J. Moreira:** Writing – review & editing, Validation, Methodology. **Luana C. Antonio:** Writing – review & editing, Validation, Methodology, Investigation. **Juliana Cancino-Bernardi:** Writing – review & editing, Supervision. **Valtencir Zucolotto:** Writing – review & editing, Supervision, Funding acquisition.

Declaration of competing interest

The authors declare that they have no known competing financial interests or personal relationships that could have appeared to influence the work reported in this paper.

Acknowledgements

LR was supported with an Abel Tasman Talent Program scholarship by the Graduate School of Medical Sciences of the University Medical Center Groningen (GSMS-UMCG). This study was financed in part by the Coordenação de Aperfeiçoamento de Pessoal de Nível Superior - Brasil (CAPES) - Finance Code 001, LR. The authors acknowledge the Brazilian Nanotechnology National Laboratory (LNNano) for the free use of their facilities (TEM-25248). PMPL was supported by the São Paulo Research Foundation (FAPESP) (Grant numbers 2017/21869-6 and 2020/00124-5). VZ is thankful to FAPESP (project number 2020/00124-5) and by the Brazilian National Council for Scientific and Technological Development (CNPq) (project number 442690/2020-7).

Appendix A. Supplementary data

Supplementary data to this article can be found online at https://doi.org/10.1016/j.bioadv.2025.214420.

Data availability

Data will be made available on request.

References

[1] J. Cheng, B.A. Teply, I. Sherifi, J. Sung, G. Luther, F.X. Gu, E. Levy-Nissenbaum, A. F. Radovic-Moreno, R. Langer, O.C. Farokhzad, Formulation of functionalized PLGA–PEG nanoparticles for in vivo targeted drug delivery, Biomaterials 28 (5) (2007) 869–876, https://doi.org/10.1016/j.biomaterials.2006.09.047.

[2] J. Chang, A. Paillard, C. Passirani, M. Morille, J.-P. Benoit, D. Betbeder, E. Garcion, Transferrin adsorption onto PLGA nanoparticles governs their interaction with

biological systems from blood circulation to brain cancer cells, Pharm. Res. 29 (6) (2012) 1495–1505, https://doi.org/10.1007/s11095-011-0624-1.
[3] A. Fuhrmann, A. Banisadr, P. Beri, T.D. Tlsty, A.J. Engler, Metastatic state of cancer cells may be indicated by adhesion strength, Biophys. J. 112 (4) (2017) 736–745, https://doi.org/10.1016/j.bpj.2016.12.038.
[4] P. Gassmann, J. Haier, G.L. Nicolson, in: H.E. Kaiser, A. Nasir (Eds.), Cell Adhesion and Invasion During Secondary Tumor Formation: Interactions Between Tumor Cells and Host Organs BT - Selected Aspects of Cancer Progression: Metastasis, Apoptosis and Immune Response, Springer Netherlands, Dordrecht, 2008, pp. 21–32, https://doi.org/10.1007/978-1-4020-6729-7_3.
[5] Y. Zhang, K. Cai, C. Li, Q. Guo, Q. Chen, X. He, L. Liu, Y. Zhang, Y. Lu, X. Chen, T. Sun, Y. Huang, J. Cheng, C. Jiang, Macrophage-membrane-coated nanoparticles for tumor-targeted chemotherapy, Nano Lett. 18 (3) (2018) 1908–1915, https://doi.org/10.1021/acs.nanolett.7b05263.
[6] C. Gao, Z. Lin, Z. Wu, X. Lin, Q. He, Stem-cell-membrane camouflaging on near-infrared photoactivated upconversion nanoarchitectures for in vivo remote-controlled photodynamic therapy, ACS Appl. Mater. Interfaces 8 (50) (2016) 34252–34260, https://doi.org/10.1021/acsami.6b12865.
[7] P.-Y. Lai, R.-Y. Huang, S.-Y. Lin, Y.-H. Lin, C.-W. Chang, Biomimetic stem cell membrane-camouflaged iron oxide nanoparticles for theranostic applications, RSC Adv. 5 (119) (2015) 98222–98230, https://doi.org/10.1039/C5RA17447C.
[8] W. Gao, C.-M.J. Hu, R.H. Fang, B.T. Luk, J. Su, L. Zhang, Surface functionalization of gold nanoparticles with red blood cell membranes, Adv. Mater. 25 (26) (2013) 3549–3553, https://doi.org/10.1002/adma.201300638.
[9] L. Rossi, A. Fraternale, M. Bianchi, M. Magnani, Red blood cell membrane processing for biomedical applications, Front. Physiol. (2019) 1070, https://doi.org/10.3389/fphys.2019.01070.
[10] D.-M. Zhu, W. Xie, Y.-S. Xiao, M. Suo, M.-H. Zan, Q.-Q. Liao, X.-J. Hu, L.-B. Chen, B. Chen, W.-T. Wu, L.-W. Ji, H.-M. Huang, S.-S. Guo, X.-Z. Zhao, Q.-Y. Liu, W. Liu, Erythrocyte membrane-coated gold nanocages for targeted photothermal and chemical cancer therapy, Nanotechnology 29 (8) (2018) 84002, https://doi.org/10.1088/1361-6528/aa9ca1.
[11] R.H. Fang, C.-M.J. Hu, B.T. Luk, W. Gao, J.A. Copp, Y. Tai, D.E. O'Connor, L. Zhang, Cancer cell membrane-coated nanoparticles for anticancer vaccination and drug delivery, Nano Lett. 14 (4) (2014) 2181–2188, https://doi.org/10.1021/nl500618u.
[12] A. Pasto, F. Giordano, M. Evangelopoulos, A. Amadori, E. Tasciotti, Cell membrane protein functionalization of nanoparticles as a new tumor-targeting strategy, Clin. Transl. Med. 8 (1) (2019) 8, https://doi.org/10.1186/s40169-019-0224-y.
[13] V.S. Marangoni, J. Cancino Bernardi, I.B. Reis, W.J. Fávaro, V. Zucolotto, Photothermia and activated drug release of natural cell membrane coated plasmonic gold nanorods and β-lapachone, ACS Appl. Bio Mater. 2 (2) (2019) 728–736, https://doi.org/10.1021/acsabm.8b00603.
[14] H. Zhang, S. Dong, Z. Li, X. Feng, W. Xu, C.M.S. Tulinao, Y. Jiang, J. Ding, Biointerface engineering nanoplatforms for cancer-targeted drug delivery, Asian J. Pharm. Sci. (2019), https://doi.org/10.1016/j.ajps.2019.11.004.
[15] Y. Zhai, J. Su, W. Ran, P. Zhang, Q. Yin, Z. Zhang, H. Yu, Y. Li, Preparation and application of cell membrane-camouflaged nanoparticles for cancer therapy, Theranostics 7 (10) (2017) 2575–2592, https://doi.org/10.7150/thno.20118.
[16] P.M. Pincela Lins, L. Ribovski, L. Corsi Antonio, W.F. Altei, H. Sobreiro Selistre-de-Araújo, J. Cancino-Bernardi, V. Zucolotto, Comparing extracellular vesicles and cell membranes as biocompatible coatings for gold nanorods: implications for targeted theranostics, Eur. J. Pharm. Biopharm. 176 (2022) 168–179, https://doi.org/10.1016/j.ejpb.2022.05.018.
[17] L. Liu, X. Bai, M.-V. Martikainen, A. Kårlund, M. Roponen, W. Xu, G. Hu, E. Tasciotti, V.-P. Lehto, Cell membrane coating integrity affects the internalization mechanism of biomimetic nanoparticles, Nat. Commun. 12 (1) (2021) 5726, https://doi.org/10.1038/s41467-021-26052-x.
[18] C.-M.J. Hu, L. Zhang, S. Aryal, C. Cheung, R.H. Fang, L. Zhang, Erythrocyte membrane-camouflaged polymeric nanoparticles as a biomimetic delivery platform, Proc. Natl. Acad. Sci. 108 (27) (2011) 10980–10985, https://doi.org/10.1073/pnas.1106634108.
[19] R.L. Siegel, K.D. Miller, A. Jemal, Cancer statistics, 2019, CA Cancer J. Clin. 69 (1) (2019) 7–34, https://doi.org/10.3322/caac.21551.
[20] R.L. Siegel, K.D. Miller, H.E. Fuchs, A. Jemal, Cancer statistics, 2022, CA Cancer J. Clin. 72 (1) (2022) 7–33, https://doi.org/10.3322/caac.21708.
[21] U. Dafni, Z. Tsourti, I. Alatsathianos, Breast Cancer statistics in the European Union: incidence and survival across European countries, Breast Care 14 (6) (2019) 344–353, https://doi.org/10.1159/000503219.
[22] H. Fessi, F. Puisieux, J.Ph. Devissaguet, N. Ammoury, S. Benita, Nanocapsule formation by interfacial polymer deposition following solvent displacement, Int. J. Pharm. 55 (1) (1989) R1–R4, https://doi.org/10.1016/0378-5173(89)90281-0.
[23] J. Schindelin, I. Arganda-Carreras, E. Frise, V. Kaynig, M. Longair, T. Pietzsch, S. Preibisch, C. Rueden, S. Saalfeld, B. Schmid, J.-Y. Tinevez, D.J. White, V. Hartenstein, K. Eliceiri, P. Tomancak, A. Cardona, Fiji: an open-source platform for biological-image analysis, Nat. Methods 9 (7) (2012) 676–682, https://doi.org/10.1038/nmeth.2019.
[24] P. Mereghetti, P.A. Corsetto, A. Cremona, A.M. Rizzo, S.M. Doglia, D. Ami, A Fourier transform infrared spectroscopy study of cell membrane domain modifications induced by docosahexaenoic acid, Biochim. Biophys. Acta Gen. Subj. 1840 (10) (2014) 3115–3122, https://doi.org/10.1016/j.bbagen.2014.07.003.
[25] L. Liu, D. Pan, S. Chen, M.-V. Martikainen, A. Kårlund, J. Ke, H. Pulkkinen, H. Ruhanen, M. Roponen, R. Käkelä, W. Xu, J. Wang, V.-P. Lehto, Systematic design of cell membrane coating to improve tumor targeting of nanoparticles, Nat. Commun. 13 (1) (2022) 6181, https://doi.org/10.1038/s41467-022-33889-3.
[26] G. Spizzo, D. Fong, M. Wurm, C. Ensinger, P. Obrist, C. Hofer, G. Mazzoleni, G. Gastl, P. Went, EpCAM expression in primary tumour tissues and metastases: an immunohistochemical analysis, J. Clin. Pathol. (2011), https://doi.org/10.1136/jcp.2011.090274.
[27] N.V. Sankpal, T.P. Fleming, P.K. Sharma, H.J. Wiedner, W.E. Gillanders, A double-negative feedback loop between EpCAM and ERK contributes to the regulation of epithelial–mesenchymal transition in cancer, Oncogene 36 (26) (2017) 3706–3717, https://doi.org/10.1038/onc.2016.504.
[28] D. Maetzel, S. Denzel, B. Mack, M. Canis, P. Went, M. Benk, C. Kieu, P. Papior, P. A. Baeuerle, M. Munz, O. Gires, Nuclear Signalling by tumour-associated antigen EpCAM, Nat. Cell Biol. 11 (2) (2009) 162–171, https://doi.org/10.1038/ncb1824.
[29] C. Reily, T.J. Stewart, M.B. Renfrow, J. Novak, Glycosylation in health and disease, Nat. Rev. Nephrol. 15 (6) (2019) 346–366, https://doi.org/10.1038/s41581-019-0129-4.
[30] X. Xi, J. Wang, Y. Qin, W. Huang, Y. You, J. Zhan, Glycosylated modification of MUC1 maybe a new target to promote drug sensitivity and efficacy for breast cancer chemotherapy, Cell Death Dis. 13 (8) (2022) 708, https://doi.org/10.1038/s41419-022-05110-2.
[31] M. Hane, K. Kitajima, C. Sato, Comprehensive analysis of oligo/polysialylglycoconjugates in cancer cell lines, Int. J. Mol. Sci. 23 (10) (2022), https://doi.org/10.3390/ijms23105569.
[32] K. Kamath, L. Wilson, F. Cabral, M.A. Jordan, BIII-tubulin induces paclitaxel resistance in association with reduced effects on microtubule dynamic instability*, J. Biol. Chem. 280 (13) (2005) 12902–12907, https://doi.org/10.1074/jbc.M414477200.
[33] H. Xiao, P. Verdier-Pinard, N. Fernandez-Fuentes, B. Burd, R. Angeletti, A. Fiser, S. B. Horwitz, G.A. Orr, Insights into the mechanism of microtubule stabilization by taxol, Proc. Natl. Acad. Sci. 103 (27) (2006) 10166–10173, https://doi.org/10.1073/pnas.0603704103.
[34] L. Rao, G.-T. Yu, Q.-F. Meng, L.-L. Bu, R. Tian, L.-S. Lin, H. Deng, W. Yang, M. Zan, J. Ding, A. Li, H. Xiao, Z.-J. Sun, W. Liu, X. Chen, Cancer cell membrane-coated nanoparticles for personalized therapy in patient-derived xenograft models, Adv. Funct. Mater. 29 (51) (2019) 1905671, https://doi.org/10.1002/adfm.201905671.
[35] R.D. Hume, S. Pensa, E.J. Brown, P.A. Kreuzaler, J. Hitchcock, A. Husmann, J. J. Campbell, A.O. Lloyd-Thomas, R.E. Cameron, C.J. Watson, Tumour cell invasiveness and response to chemotherapeutics in adipocyte invested 3D engineered anisotropic collagen scaffolds, Sci. Rep. 8 (1) (2018) 12658, https://doi.org/10.1038/s41598-018-30107-3.
[36] M.J. Bissell, D.C. Radisky, A. Rizki, V.M. Weaver, O.W. Petersen, The organizing principle: microenvironmental influences in the normal and malignant breast, Differentiation 70 (9–10) (2002) 537–546, https://doi.org/10.1046/j.1432-0436.2002.700907.x.
[37] A. Labernadie, T. Kato, A. Brugués, X. Serra-Picamal, S. Derzsi, E. Arwert, A. Weston, V. González-Tarragó, A. Elosegui-Artola, L. Albertazzi, J. Alcaraz, P. Roca-Cusachs, E. Sahai, X. Trepat, A mechanically active heterotypic E-cadherin/N-cadherin adhesion enables fibroblasts to drive cancer cell invasion, Nat. Cell Biol. 19 (3) (2017) 224–237, https://doi.org/10.1038/ncb3478.
[38] M. Apostolopoulou, L. Ligon, Cadherin-23 mediates heterotypic cell-cell adhesion between breast cancer epithelial cells and fibroblasts, PLoS One 7 (3) (2012) e33289.
[39] O. Ilina, P.G. Gritsenko, S. Syga, J. Lippoldt, C.A.M. La Porta, O. Chepizhko, S. Grosser, M. Vullings, G.-J. Bakker, J. Starruß, P. Bult, S. Zapperi, J.A. Käs, A. Deutsch, P. Friedl, Cell–cell adhesion and 3D matrix confinement determine jamming transitions in breast cancer invasion, Nat. Cell Biol. 22 (9) (2020) 1103–1115, https://doi.org/10.1038/s41556-020-0552-6.
[40] M.V. Plikus, X. Wang, S. Sinha, E. Forte, S.M. Thompson, E.L. Herzog, R.R. Driskell, N. Rosenthal, J. Biernaskie, V. Horsley, Fibroblasts: origins, definitions, and functions in health and disease, Cell 184 (15) (2021) 3852–3872, https://doi.org/10.1016/j.cell.2021.06.024.
[41] L.C. Antonio, L. Ribovski, P.M. Pincela Lins, V. Zucolotto, The amount of dextran in PLGA Nanocarriers modulates protein corona and promotes cell membrane damage, J. Mater. Chem. B (2022), https://doi.org/10.1039/D2TB01296K.
[42] G. Batist, G. Ramakrishnan, C.S. Rao, A. Chandrasekharan, J. Gutheil, T. Guthrie, P. Shah, A. Khojasteh, M.K. Nair, K. Hoelzer, K. Tkaczuk, Y.C. Park, L.W. Lee, Reduced cardiotoxicity and preserved antitumor efficacy of liposome-encapsulated doxorubicin and cyclophosphamide compared with conventional doxorubicin and cyclophosphamide in a randomized, multicenter trial of metastatic breast Cancer, J. Clin. Oncol. 19 (5) (2001) 1444–1454, https://doi.org/10.1200/JCO.2001.19.5.1444.
[43] L. Belyanskaya, P. Manser, P. Spohn, A. Bruinink, P. Wick, The reliability and limits of the MTT reduction assay for carbon nanotubes-cell interaction, Carbon N Y 45 (13) (2007) 2643–2648, https://doi.org/10.1016/j.carbon.2007.08.010.